Journal of Alloys and Compounds 519 (2012) 72–76

Contents lists available at SciVerse ScienceDirect

Journal of Alloys and Compounds

journal homepage: www.elsevier.com/locate/jallcom

The effects of hydrothermal temperature on structural and photocatalytic properties of ordered large pore size TiO_2–SiO_2 mesostructured composite

Babak Mazinani[a,b,*], Ali Beitollahi[a], Shahidan Radiman[c], Abdul Kadir Masrom[b], Suhaina Mohd Ibrahim[b], Jafar Javadpour[a], Farina M.D. Jamil[b]

[a] Center of Excellence on Processing of Advanced Materials, School of Metallurgy and Materials Engineering, Iran University of Science and Technology (IUST), Tehran, Iran
[b] Industrial Nanotechnology Research Center, C/O AMREC, Lot 34, Jalan Hi-Tech Park, 09000 Kulim, Kedah, Malaysia
[c] School of Applied Physics, Faculty of Science and Technology, Universiti Kebangsaan Malaysia, 43600 UKM, Bangi, Selangor, Malaysia

ARTICLE INFO

Article history:
Received 18 October 2011
Received in revised form 6 December 2011
Accepted 12 December 2011
Available online 8 January 2012

Keywords:
Oxide materials
Chemical synthesis
Photocatalytic properties
Mesoporous materials

ABSTRACT

Ordered TiO_2–SiO_2 mesoporous materials with BJH pore diameters in the range from 12 to 15 nm were synthesized by a one-step hydrothermal synthesis method. In this route, tetraethoxysilane (TEOS) and titanium tetraisopropoxide (TTIP) in a low pH solution were used as SiO_2 and TiO_2 precursor, respectively with P123 as a template and hexane as a micelle expander in the presence of NH_4F. In this work, we show the effect of different hydrothermal temperatures (70 °C and 130 °C) on pore structure and photocatalytic efficiency of the materials prepared. The synthesized materials were characterized by small-angle X-ray scattering (SAXS), N_2 adsorption–desorption experiments, X ray diffraction (XRD), X-ray photoelectron spectroscopy (XPS) and field emission scanning electron microscopy (FESEM). The method could produce ordered mesoporous structure with uniform pore size of 12–15 nm and high specific surface areas S_{BET} up to 431 m^2/g. The photocatalytic activity of the samples was evaluated by degradation of MB under UV light irradiation and results showed these mesostructure materials have much higher photocatalytic efficiency in comparison with commercial P25 titania. The results also show that for materials synthesized using higher hydrothermal temperature (130 °C) resulting in increased in photocatalytic activity due to higher formation of anatase phase and more open channels by comparison with lower hydrothermal treatment (70 °C).

1. Introduction

TiO_2 as a photocatalyst has attracted much attention due to its high chemical stability, low price and nontoxicity [1–5]. Nevertheless, limited photocatalytic activity of TiO_2 is one of the reasons for their limited industrial usage. Photocatalytic properties of TiO_2 are greatly dependent on their physicochemical properties. Decreasing the size of TiO_2 particles will significantly increase surface area and enhanced photocatalytic efficiency [6,7]. However, difficulties encountered in separation of fine size TiO_2 particles become the major obstacle for large scale industrial applications. In order to overcome this problem and to further improve photocatalytic activity, development of TiO_2 having mesoporous structure became a good alternative as this structure will provide abundant pores and large surface area [8–10]. However there are several process limitations in preparing mesoporous titania, such as high hydrolysis and condensation rates of Ti-precursors [11–13] and phase transformation from anatase to rutile around 500–700 °C [14–19], that make process control difficult. Due to the above mentioned difficulties for preparing mesoporous TiO_2, many attempts have been done to activate a mesoporous silica material with titania. The activation can be carried out by impregnation of TiO_2 particles inside the pores of pre-synthesized mesoporous silica [20–24], whereby possible blocking of the pores occurs [25]. Another route to prepare SiO_2–TiO_2 mesoporous materials is by introduction of Ti source during synthesis of mesoporous silica [26–31]. As we show in this study, although, photocatalytic performance and physical properties of composite are affected by hydrothermal temperature; there are no similar work reported in the literature. On the other hand, the outcome from our investigation could lead to many potential applications as many other compounds can be impregnated into the large pores including incorporation of semiconductor compounds in order to improve the photocatalytic activity of TiO_2 [32,33].

In this article, we report the preparation of ordered TiO_2–SiO_2 Mesostructured composite having large pore sizes of between 12 and 15 nm. We report the influence of two different hydrothermal temperatures (70 °C and 130 °C) on the structure of pores and photocatalytic activity of mesoporous TiO_2–SiO_2 composite.

* Corresponding author at: N 45, Gholami St., Shabestari St., 196 Sharghi St., Tehranpars, Tehran, Iran. Tel.: +60 194090948/+98 9122935223; fax: +98 2166734510.
E-mail addresses: b.mazinani@gmail.com, b_mazinany@iust.ac.ir (B. Mazinani).

0925-8388/$ – see front matter © 2011 Elsevier B.V. All rights reserved.
doi:10.1016/j.jallcom.2011.12.051

2. Materials and methods

2.1. Materials

Pluronic triblock copolymer P123 poly(ethylene glycol)–poly(propylene glycol)–poly(ethylene glycol), M_w = 5800 and titanium tertaisopropoxide (TTIP) were purchased from Aldrich. Tetraethoxysilane (TEOS), NH_4F and HCl (37% concentration) were purchased from Merck. Hexane was bought from Baker (≥99% purity).

2.2. Synthesis

In a typical synthesis, 2.4 g of P123 was dissolved in 84 ml HCl solution (1.3 M), followed by the addition of 0.027 g of NH_4F. The mixture was stirred at room temperature for 3 h. Subsequently, the solution was transferred to a water bath (temperature accuracy of 0.1 °C) set at 15 °C, and after 2 h, a mixture of 5.5 ml TEOS and 15 ml hexanes were introduced. Thereafter, TTIP was added drop wise to the aqueous solution (weight ratio of SiO_2/TiO_2 = 2) under stirring. The solution was stirred for 24 h at 15 °C, and then transferred into an autoclave for further reaction at 70 °C and 130 °C for 48 h (T70 and T130 samples, respectively). The precipitate was filtered, washed and dried. Finally, calcination was carried out in air by increasing the temperature from room temperature (25 °C) to 540 °C with a heating rate of 5 °C/min, and holding for 14 h at 550 °C. Next the temperature was increased to 800 °C and heated for 3 h.

2.3. Characterization

Small-angle X-ray scattering (SAXS) measurements were performed on a Kratky compact small-angle system using Kα radiation at 40 kV and 20 mA, which equipped with a position-sensitive detector containing 1024 channels of width 53.0 mm. After degassing of sample at 250 °C for 6 h, the surface area was measured by using nitrogen absorption–desorption (BET)-Autosorb-1 from Quantachrome instruments. XRD patterns were recorded with a Bruker powder X-ray diffractometer using a Cu radiation source of wavelength 1.54 Å ranging from 20° to 80° with a scan speed of 0.04°/s at 40 kV and 40 mA. The morphology of the samples was characterized by SEM (LEO-1525) with an accelerating voltage of 20 kV. X-ray photoelectron spectroscopy (XPS) spectra were recorded with Omicron Nanotechnology (ELS5000) system using Al Kα radiation at a base pressure below 5.5×10^{-9} Torr.

2.4. Photocatalytic activity measurement

The photocatalytic activity of the prepared samples was evaluated by measuring the degradation of methylene blue (MB) dye in aqueous solution under UV light irradiation (mercury lamp 125 W). In a typical experiment, 30 mg of commercial pure TiO_2 (P25, Degussa Co., Germany) was dispersed in 100 ml of MB solutions having a concentration 40 mg/l. The amounts of TiO_2/SiO_2 materials were estimated to achieve the same TiO_2 loading. The mixture was first stirred for 30 min in dark condition. The concentration spectrum of the mixture was determined using UV–vis spectrometer (in 625 nm wavelength) after centrifuging.

3. Results and discussion

The SAXS profiles of prepared samples are displayed in Fig. 1. Both of them exhibit three peaks that can be indexed to the (1 0 0), (1 1 0) and (2 0 0) reflections associated with a 2-D hexagonal structure. The 2D hexagonal pore arrays are confirmed by FESEM images (Fig. 5). The (1 1 0) reflection reveals a more intense peak for the sample treated at 130 °C due to thinner walls (Table 1) as shown by others [34,35]. From the SAXS results, the *d* spacing and hexagonal

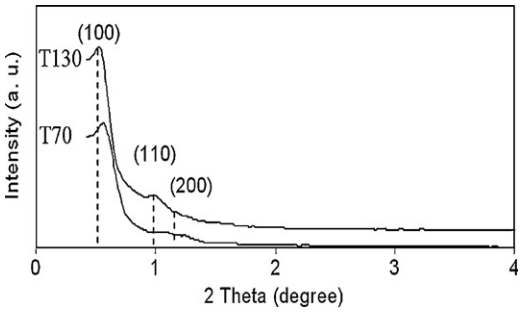

Fig. 1. SAXS pattern of the samples.

unit-cell dimension (a_0) were calculated (Table 1). It was observed that increasing the hydrothermal temperature from 70 °C to 130 °C led to growing lattice parameter of sample which it can be due to incomplete condensation at low hydrothermal temperature as suggested in other reports for SBA-15 [36].

The N_2 adsorption–desorption isotherms and the corresponding pore size distribution calculated from the adsorption branch of N_2 isotherm can be seen in Fig. 2a and b, respectively.

It is clear that the hydrothermal temperature can modify structural properties of the synthesized samples as shown by the changes of the hysteresis loops of the samples isotherm (Fig. 2 and Table 1). The isotherms can be classified as type IV according to IUPAC. In the case of low hydrothermal sample (L70), results show existence of a broad hysteresis loop starting around P/P_0 = 0.4 indicate the narrowing of pores channel or plugging of its cylindrical pores [37]. Similar broad hysteresis has been reported for pure mesoporous SiO_2 expanded by hexane for non-hydrothermal samples [38]. As the rate of hydrolysis of TEOS can be affected significantly by temperature and its polymerization and condensation rates are rather slow at low temperature [39], incomplete hydrolysis of compounds in the hydrophobic poly (propylene oxide) (PPO) cores of micelles (PPO-solubilized TEOS) can be the reason of blocked pores. In the other words, the non-hydrolyzed or incompletely hydrolyzed TEOS can transform to siliceous framework during calcinations, forming blockage inside the channels [38,40]. As the hydrothermal temperature increases to 130 °C, a narrow hysteresis loop at high pressure with clear H1 hysteresis (Fig. 2a) was obtained indicating present of large and open pores. As reported by others [41], higher hydrothermal temperature results in formation of larger pores, higher pore volume and lower surface area. Structural parameters of the samples are shown in Table 1 shows wall shrinkage (30.4%) by increment in hydrothermal temperature from 70 °C to 130 °C.

XRD was performed to investigate the structural phases and crystallite size of the samples. Fig. 3 shows the XRD patterns of the samples. A mixed crystal structure containing anatase and rutile can be seen for both of them. The weight fractions of the anatase

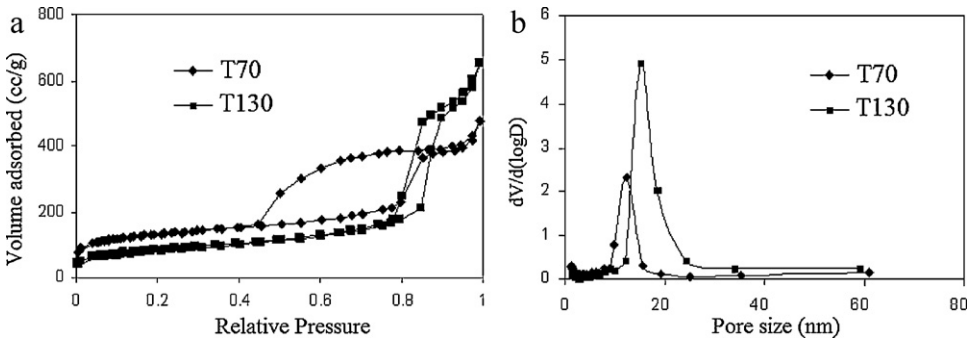

Fig. 2. (a) Nitrogen sorption isotherms and (b) pore size distribution calculated from adsorption branch of the samples.

Table 1
Structural parameters of the samples.

Sample ID	d_{100} spacing (nm)	a (nm)[a]	S_{BET} (m^2/g)[b]	D (nm)[c]	V_p (cc/g)[d]	t (nm)[e]
T70	15.3	17.7	431.7	12.4	0.7	5.3
T130	16.3	18.8	281.3	15.1	1	3.7

[a] Cell parameter.
[b] BET surface area.
[c] BJH pore diameter calculated from adsorption branch of the isotherm.
[d] Adsorption total pore volume.
[e] Wall thickness ($t = a - D$).

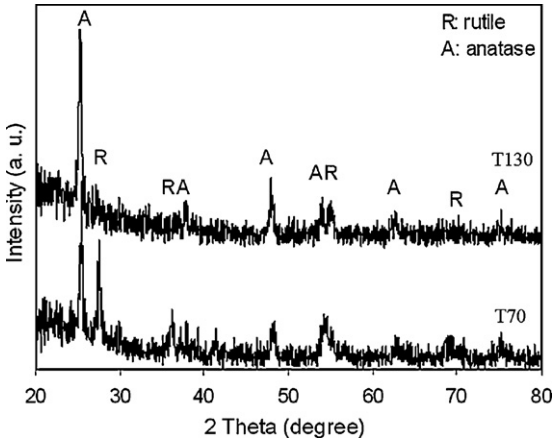

Fig. 3. XRD patterns of samples.

(W_A) and rutile (W_R) phases in the samples were calculated from the relative intensities of the strongest peaks corresponding to anatase and rutile as described by Spurr and Myers [42]:

$$W_R = \frac{1}{1 + 0.8(I_A/I_R)} \quad (1)$$

where I_A and I_R are the X-ray integrated intensities of the (1 0 1) reflection of anatase and (1 1 0) reflection of rutile, respectively. The calculated weight percentage of rutile and anatase phase using Eq. (1) and corresponding crystallite size calculated by Scherrer's equation [43] are summarized in Table 2.

In the case of T70, high amount of rutile (46.5%) was found while at higher hydrothermal temperature (sample T130) the major phase is anatase (Table 1). Both anatase and rutile consist of tetragonal structures having $[TiO_6]^{2-}$ octahedral, which share edges and corners in different ways while keeping the overall stoichiometry as TiO_2. In rutile two opposite edges of each $[TiO_6]^{2-}$ octahedra are shared to form a linear chain and these chains are further linked to each other by sharing the corner oxygen atoms, but in anatase four edges of the $[TiO_6]^{2-}$ octahedra are shared. The linear arrangement is the most stable structure since the electrostatic repulsive energy is minimized, thus thermodynamically, the basic structure of rutile is favored. The higher energy upon collision at 90 °C enables the octahedrons to overcome the electrostatic repulsion and form anatase phase [44–50].

Table 2
Calculated weight percentages of rutile and anatase and their corresponding crystallite sizes.

Sample	Anatase phase		Rutile phase	
	Wt%	Crystallite size (nm)	Wt%	Crystallite size (nm)
T70	53.5	33.1	46.5	26.5
T130	73.5	31.6	26.5	25

To obtain the information about titanium coordination state in the synthesized samples, X-ray photoelectron spectroscopy (XPS) analyses were performed for both samples.

From Fig. 4a and b, the profiles of the samples can be fit by three Lorentzian curves. The peaks around 532 eV and 530 eV are assigned to oxygen in Si—O—Si and Ti—O—Ti bonds, respectively. In addition, a peak at an intermediate binding energy (531 eV) could be assigned to oxygen in Si—O—Ti [51]. It has been mentioned that the existence of Ti—O—Si bond can improve photocatalytic activity due to increase of surface acidity in the samples [52].

Fig. 5 presents the FESEM micrograph of T70 (a–c) and T130 (d–f). Low magnification patterns (Fig. 5a and d) show the overall morphology for both of the samples exhibit rod-like shape with the length approximately about 50 nm. Although there are some limitations for getting a very clear view of pores by FESEM, ordered honeycomb pore structure can be seen in high magnification FESEM pictures which confirm LAXRD results (Fig. 5c and f). On the other hand average pore size was estimated to be in the range of 12–16 nm which support BJH results (Table 1).

Methylene blue as a toxic, carcinogenic and non-biodegradable material can be decomposed by crystalline titania in the presence of UV light in aqueous solution. After activation of TiO_2 by photon, the electrons excite from the valence band to conduction band which leads the formation of negatively charged electrons and positive holes. The positive holes in valence band can gain electrons from species such as water; resulting in the formation of hydroxyl radical which is a strong oxidizing agent. Dyes like MB can be oxidized directly or through intermediate compounds by hydroxyl radicals [53].

The photocatalytic activities of the prepared samples were tested by the degradation of methylene blue (MB) dye as model reaction in the presence of UV light in aqueous solution and the results of photocatalytic and kinetics study are shown in Fig. 6a and b, respectively. As it can be seen Si–Ti system increase the photocatalytic activity in comparison with commercial P25 titania. The rate of degradation was assumed to obey pseudo-first-order kinetics and the initial reaction rate constants were calculated according to the formula $-\mathrm{Ln}(C/C_0) = kt$, where C/C_0 is the normalized organic compounds concentration and k is the apparent reaction rate constant.

The activity of titania will depend on several parameters, including electron–hole recombination, number of electrons created, phase composition (anatase or rutile), surface area, crystallinity, size of TiO_2 and the absorption properties of the dyes on the surface of TiO_2 used [54,55]. Two factors can be mentioned for decreasing of concentration of MB in photodegradation experiments, (i) the adsorption of MB onto the surface of photocatalyst and (ii) photodegradation of MB. In order to evaluate each of them the suspension was initially stirred for 30 min in dark condition. As the adsorption of MB in dark condition is related to surface area, MB reductions are directly related to the adsorption of MB onto the surface of the photocatalyst materials [56]. Thus, in the case of P25, MB reduction cannot be recognized due to low surface area of P25.

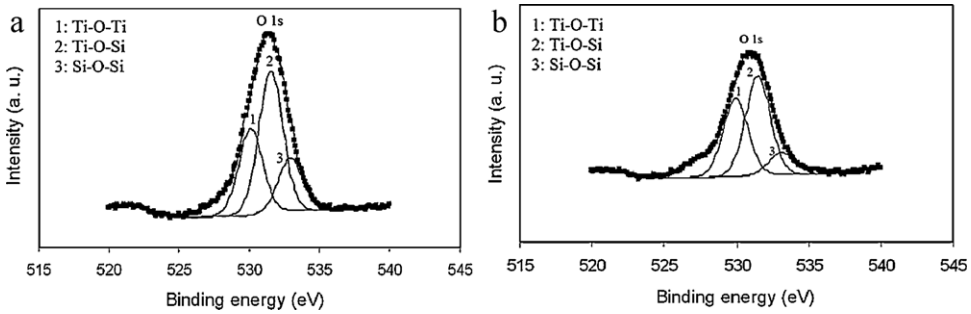

Fig. 4. XPS spectra of: (a) T70 and (b) T130 sample focus on the O1s region.

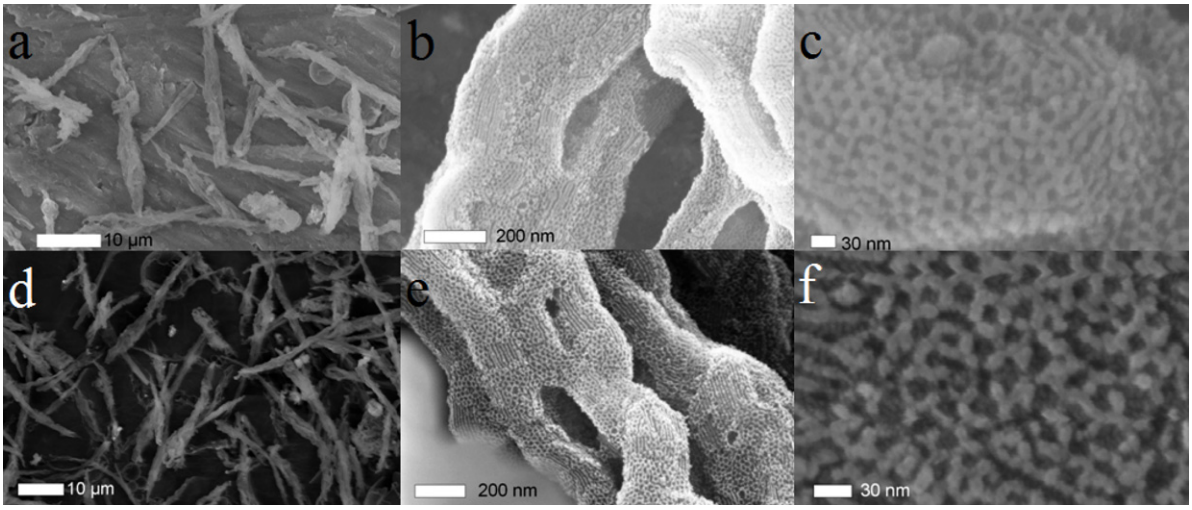

Fig. 5. FESEM images of: T70 (a–c) and T130 (d–f).

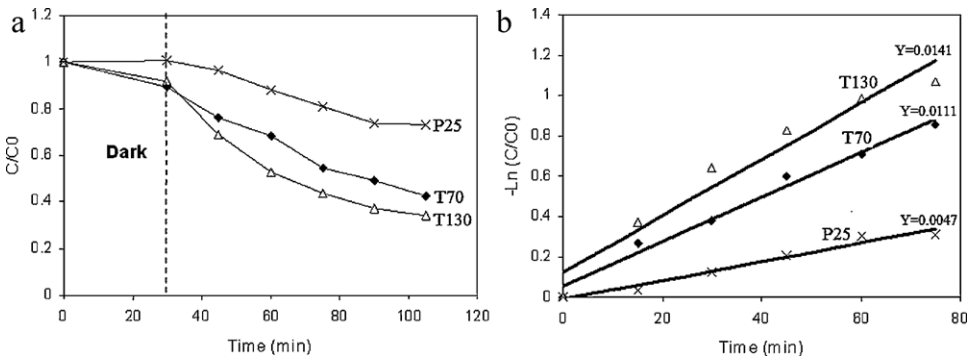

Fig. 6. (a) UV light photodegradation effect of MB and (b) the photodegradation kinetic curve in the presence of P25, T70 and T130.

Results in Fig. 6 clearly show both TiO_2–SiO_2 mesoporous materials exhibit superior photodegredation of MB than P25 commercial materials with T130 exhibited higher efficiency than T70. This photocatalytic activity results can be related to high surface area of mesoporous materials and the existence of Ti—O—Si chemical bonds which improve photocatalytic properties in comparison with P25. On the other hand, although the sample hydrothermal at lower temperature (70 °C) has much higher surface area (Table 1), higher hydrothermal temperature (130 °C) improves photodegradation (Fig. 6). This interesting phenomenon of enhancement of photocatalytic performance can be related to higher amount of anatase phase in T130 sample according to XRD results (Fig. 3 and Table 2) and present of more open and accessible channels for materials prepared with higher hydrothermal temperature (Fig. 2a). The calculated rate constant of samples after dark condition show the highest amount for T130 ($K = 0.014\ min^{-1}$) in Fig. 6b.

4. Conclusion

In summary, we successfully synthesized ordered mesoporous TiO_2–SiO_2 with large pores (12–15 nm) by introducing TTIP as Ti source and hexane as micelle expander into solution at low synthesis temperature ($T = 15$ °C). The results showed that hydrothermal temperature has a strong effect on the physical properties and with enhanced photocatalytic performance of the sample. Although, high hydrothermal temperature (130 °C) leads to lower surface area but with higher amount of anatase phase and more open and

accessible pores can be achieved in comparison with materials prepared with hydrothermal temperature of 70 °C.

Acknowledgments

This work was supported by the SIRIM Bhd and Iran University of Science and Technology (IUST) through joint research within these two institutions. The authors are also grateful to faculty of Applied Science, Universiti Kebangsaan Malaysia for their kind assistance in performing some of the characterization works.

References

[1] M.R. Hoffmann, S.T. Martin, W.Y. Choi, D.W. Bahnemann, Chem. Rev. 95 (1995) 69.
[2] A. Fujishima, N.T. Rao, D.A. Rryk, J. Photochem. Photobiol. C: Rev. 1 (2000) 1.
[3] Y. Zhao, C. Li, X. Liu, F. Gu, J. Alloys Compd. 440 (2007) 281.
[4] H. Xia, H. Zhuang, D. Xiao, T. Zhang, J. Alloys Compd. 465 (2008) 328.
[5] Y. Yan, X. Qiu, H. Wang, L. Li, X. Fu, L. Wu, G. Li, J. Alloys Compd. 460 (2008) 491.
[6] N. Xu, Z. Shi, Y. Fan, J. Dong, J. Shi, Z.-C. Hu, Ind. Eng. Chem. Res. 38 (1999) 373.
[7] B. Ohtani, Y. Ogawa, S. i. Nishimoto, J. Phys. Chem. B 101 (1997) 3746.
[8] A. Beitollahi, A.H. Haj Daie, L. Samie, M.M. Akbarnejad, J. Alloys Compd. 490 (2010) 311.
[9] T. An, J. Liu, G. Li, S. Zhang, H. Zhao, X. Zeng, G. Sheng, J. Fu, Appl. Catal. A 350 (2008) 237.
[10] J. Du, Z. Liu, Z. Li, B. Han, Y. Huang, Y. Gao, Micropor. Mesopor. Mater. 83 (2005) 19.
[11] G.J.de A.A. Soler-Illia, C. Sanchez, B. Lebeau, J. Patarin, Chem. Rev. 102 (2002) 4093.
[12] P. Yang, D. Zhao, D.I. Margolese, B.F. Chmelka, G.D. Stucky, Nature 396 (1998) 152.
[13] G.J.de A.A. Soler-Illia, A. Louis, C. Sanchez, Chem. Mater. 14 (2002) 750.
[14] B. Tian, H. Yang, X. Liu, S. Xie, C. Yu, J. Fan, B. Tu, D. Zhao, Chem. Commun. (2002) 1824.
[15] M.D. Perez, E. Otal, S.A. Bilmes, G.J. Soler-Illia, E.L. Crepaldi, D. Grosso, C. Sanchez, Langmuir 20 (2004) 6879.
[16] S.Y. Choi, B. Lee, D.B. Carew, M. Mamak, F.C. Peiris, S. Speakman, N. Chopra, G.A. Ozin, Adv. Funct. Mater. 16 (2006) 1731.
[17] H.X. Li, Z.F. Bian, J. Zhu, Y.N. Huo, H. Li, Y.F. Lu, J. Am. Chem. Soc. 129 (2007) 4538.
[18] X. Ding, X. Liu, J. Mater. Res. 139 (1998) 2556.
[19] J. Ovenstone, K. Yanagisawa, Chem. Mater. 11 (1999) 2770.
[20] E. Beyers, E. Biermans, S. Ribbens, K. De Witte, M. Mertens, V. Meynen, S. Bals, G. Van Tendeloo, E.F. Vansant, P. Cool, Appl. Catal. B: Environ. 88 (2009) 515.
[21] F. Berube, A. Khadhraoui, M.T. Janicke, F. Kleitz, S. Kaliaguine, Ind. Eng. Chem. Res. 49 (2010) 6977.
[22] Z. Luan, E.M. Maes, P.A.W. van der Heide, D. Zhao, R.S Czernszewicz, L. Kevan, Chem. Mater. 11 (1999) 3680.
[23] L. Zhao, J. Yu, J. Colloid Interface Sci. 304 (2006) 84.
[24] E. Beyers, E. Biermans, S. Ribbens, K.D. Witte, M. Mertens, V. Meynen, S. Bals, G.V. Tendeloo, E.F. Vansant, P. Cool, Appl. Catal. 84 (2008) 699.
[25] L. Vradman, M.V. Landau, D. Kantorovich, Y. Kolypin, A. Gedanken, Micropor. Mesopor. Mater. 79 (2005) 307.
[26] X. Zhang, F. Zhang, K.-Y. Chan, Appl. Catal. 284 (2005) 193.
[27] X. Zhang, H. Yang, F. Zhang, K.-Y. Chan, Mater. Lett. 61 (2007) 2231.
[28] W.T. Qiao, G.W. Zhou, X.T. Zhang, T.D. Li, Mater. Sci. Eng. C 29 (2009) 1498.
[29] J. Zou, J. Gao, J. Hazard. Mater. 185 (2011) 710.
[30] N. Yao, S. Cao, K.L. Yeung, Micropor. Mesopor. Mater. 117 (2009) 570.
[31] A. Hilonga, J.-K. Kim, P.B. Sarawade, H.T. Kim, J. Mater. Sci. 45 (2010) 1264.
[32] H. Wang, Z. Wu, Y. Liu, Z. Sheng, J. Mol. Catal. A: Chem. 287 (2008) 176.
[33] R.M. Mohamed, I.A. Mkhalid, J. Alloys Compd. 501 (2010) 143.
[34] B.P. Feuston, J.B. Higgins, J. Phys. Chem. B 98 (1994) 4459.
[35] M. Kruk, M. Jaroniec, C. Ko, R. Ryoo, Chem. Mater. 12 (2000) 1961.
[36] A. Galarneaue, H. Cambon, F.D. Renzo, R. Ryoo, M. Choi, F. Fajula, N. J. Chem. 27 (2003) 73.
[37] P. Van Der Voort, M. Benjelloun, E.F. Vansant, J. Phys. Chem. B 106 (2002) 9027.
[38] M. Kruk, L. Cao, Langmuir 23 (2007) 7247.
[39] L.-Z. Wang, J.-L. Shi, J. Yu, W.-H. Zhang, D.-S. Yan, Mater. Lett. 45 (2000) 273.
[40] D. Zhao, Q. Huo, J. Feng, B.F. Chmelka, G.D.J. Stucky, J. Am. Chem. Soc. 120 (1998) 6024.
[41] L. Chen, Y. Meng Wang, M.-Y. He, J. Porous Mater. 18 (2011) 211.
[42] R.A. Spurr, H. Myers, Anal. Chem. 29 (1957) 760.
[43] H.P. Klug, L.E. Alexander, X-ray Diffraction Procedures, Willy, New York, 1954.
[44] Q. Zhang, L. Gao, Langmuir 19 (2003) 967.
[45] C. He, B. Tian, J. Hang, Micropor. Mesopor. Mater. 126 (2009) 50.
[46] J.H. Lee, Y.S. Yang, J. Mater. Sci. 41 (2006) 557.
[47] A. Testino, I.R. Bellobono, V. Buscaglia, C. Canevali, M. D'Arienzo, S. Polizzi, R. Scotti, F. Morazzoni, J. Am. Chem. Soc. 129 (2007) 3564.
[48] S. Watson, D. Beydoun, J. Scott, R. Amal, J. Nanopart. Res. 6 (2004) 193.
[49] K. Yanagisawa, J. Ovenstone, J. Phys. Chem. B 103 (1999) 7781.
[50] P. Periyat, K.V. Baiju, P. Mukundan, P.K. Pillai, K.G.K. Warrier, Appl. Catal. 349 (2008) 13.
[51] Z.L. Hua, J.L. Shi, L.X. Zhang, M.L. Ruan, J.N. Yan, Adv. Mater. 14 (2002) 830.
[52] J.Y. Zhang, Q. Li, W.L. Cao, Inorg. Chem. 20 (2004) 725.
[53] A. Houas, H. Lachheb, M. Kisbi, E. Elaloui, C. Guillard, J.M. Hermann, Appl. Catal. B: Environ. 31 (2001) 145.
[54] Q.Z. Yan, T.S. Xin, Z.Y. Huang, C. Ge, J. Eur. Ceram. Soc 26 (2006) 915.
[55] X. Chen, Y. Lou, A.N.S. Samia, C. Burda, J.L. Gole, Adv. Funct. Mater. 15 (2005) 41.
[56] C. He, B. Tian, J. Zhang, J. Colloid Interface Sci. 344 (2010) 382.